Available online at www.sciencedirect.com
SCIENCE DIRECT
Journal of Catalysis 231 (2005) 172–180
JOURNAL OF CATALYSIS
www.elsevier.com/locate/jcat

Microkinetic modelling of the dehydrogenation of ethylbenzene to styrene over unpromoted iron oxides

Achim Schüle [a], Osama Shekhah [b], Wolfgang Ranke [b], Robert Schlögl [b], Grigorios Kolios [a,*]

[a] *Institute of Chemical Processes Engineering, University of Stuttgart, Böblinger Str. 72, D-70199 Stuttgart, Germany*
[b] *Department of Inorganic Chemistry, Fritz-Haber-Institute of the MPG, Faradayweg 4-6, D-14195 Berlin, Germany*

Received 28 June 2004; revised 20 December 2004; accepted 12 January 2005

Abstract

A vast number of surface science experiments provide a detailed qualitative picture of the mechanisms governing the catalytic dehydrogenation of ethylbenzene (EB) to styrene (St) over unpromoted iron oxide. Values of kinetic and energetic parameters for adsorption and desorption are also available. We present a methodology of kinetic modelling based upon this knowledge, aimed at producing an accurate prediction of the behaviour of the technical catalysts including, deactivation and regeneration. This paper contains a detailed kinetic model and the procedure followed for determining the kinetic parameters.

Keywords: Microkinetic model; Dehydrogenation; Ethylbenzene; Styrene; Iron oxide; Deactivation; Coking; Solid phase transformation

1. Introduction

The power of microkinetic modelling [1] of a catalytic process based on data obtained from surface science studies has already been demonstrated for ammonia synthesis [2–4] as reviewed in [5]. The catalyst in this system can be considered invariant. However, including gas–solid interactions in catalytic reaction processes usually results in a change of state of the catalyst. In most cases these solid-state transformations are connected with catalyst deactivation.

A typical example is the potassium-promoted iron oxide catalyst used for styrene synthesis through dehydrogenation of ethylbenzene. It is known that the styrene catalyst undergoes significant changes during its lifetime. This involves physical degradation, formation of carbonaceous deposits, and an inherent phase change of Fe_2O_3 (hematite) under reaction conditions towards Fe_3O_4 (magnetite), which exhibits only a minor catalytic activity [6,7]. Nevertheless, kinetic expressions published by several groups [8–10] neglect these transient effects occurring under normal operating conditions. Therefore, such standard kinetic models have clear practical restrictions. They are not suitable for describing the catalytic behaviour, except at a certain stationary state. With these methods model-based process optimisation and assessment of the potential of novel reactor concepts become infeasible [8,11,12]. The shortcomings of available kinetic models definitely affect the progress in engineering of the styrene process. Clearly, it is infeasible to resolve the mechanism of the process by studying the behaviour of the real catalyst under practically relevant conditions. The goal of analysing individual aspects isolated under well-defined conditions led to a surface science approach. This approach relies on detailed conversion measurements and analyses of gas–surface interactions for monocrystalline model surfaces [13–20]. Details of the experimental setup and of the kinetic measurements are presented in [19–21]. The most comprehensive set of experimental data so far is available for epitactically grown single crystal films (SCFs) of iron oxide representing a generic model of the real catalyst. These experiments provide intrinsic reaction rates that are not compromised by diffusional limitations; time-resolved informa-

* Corresponding author. Fax: +49/711-6412242.
E-mail address: kolios@icvt.uni-stuttgart.de (G. Kolios).

0021-9517/$ – see front matter
doi:10.1016/j.jcat.2005.01.013

tion on the changes in the film composition in the reaction atmosphere; kinetic and equilibrium parameters for the adsorption of individual components of the reaction mixture on the model surface.

The available information allows for the postulation of a qualitative mechanistic model of ethylbenzene dehydrogenation over iron oxides.

However, the final goal is to translate this information into technical conditions. A model-based approach is used to bridge the gap between the observations made on ideal surfaces and the behaviour of real catalysts. The chosen approach is based on the standard modelling procedure applied in chemical reaction engineering: the task is mainly to compute a set of parameters of the kinetic reactor model such that simulation results resemble the measured values as closely as possible. The novelty of the present contribution lies in the structure of the model and the experimental basis used for adjusting the free model parameters.

The underlying mechanistic catalyst model is introduced in Section 2 and the model equations in Section 3. Finally, parameterisation and validation of the model are discussed in Section 4.

2. Catalyst model

The primary goal of our approach is a mechanistic description of the relevant physico-chemical gas–solid-interactions during dehydrogenation of ethylbenzene to styrene over iron oxide, thus the derivation of a mechanistic catalyst model. The model is represented by a set of stoichiometric equations describing the main reaction, the redox processes, and coke formation on the catalyst surface. Side reactions towards benzene and toluene are neglected. The overall activity of the surface includes the contribution of clean iron oxide and coked areas. The model is based on the following assumptions: overall conversion is split up into individual steps of adsorption, surface reaction, and desorption; gas–solid reactions related to formation and gasification of coke and phase transformation of iron oxide are considered as single-step reactions.

Fig. 1 shows the considered reaction steps. The surface is assumed to be inhomogeneous, consisting of areas of clean iron oxide and those covered by coke. The iron oxide layer is

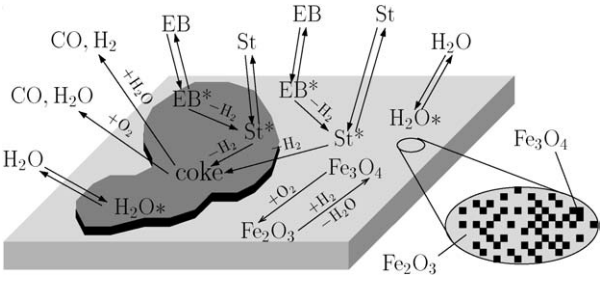

Fig. 1. Schematic representation of the mechanistic model of ethylbenzene dehydrogenation over iron oxide.

considered as a mixture of hematite and magnetite, depending on the oxygen content. The feed components water and ethylbenzene, as well as styrene, adsorb at the surface. Thermal desorption mass spectroscopy (TDS) confirms the existence of the respective surface species [17]. The adsorption-desorption equilibrium is described by the following stoichiometric equations (adsorption: Eqs. (1)–(3); desorption: Eqs. (4)–(6)):

$$\mathrm{EB} + {}^{*} \rightarrow \mathrm{EB}^{*}, \tag{1}$$

$$\mathrm{St} + {}^{*} \rightarrow \mathrm{St}^{*}, \tag{2}$$

$$\mathrm{H_2O} + {}^{*} \rightarrow \mathrm{H_2O}^{*}, \tag{3}$$

each on iron oxide and coke;

$$\mathrm{EB}^{*} \rightarrow \mathrm{EB} + {}^{*}, \tag{4}$$

$$\mathrm{St}^{*} \rightarrow \mathrm{St} + {}^{*}, \tag{5}$$

$$\mathrm{H_2O}^{*} \rightarrow \mathrm{H_2O} + {}^{*}, \tag{6}$$

each on iron oxide and coke.

Only vague information exists on the conversion of adsorbed ethylbenzene to styrene. Dehydrogenation of EB via H-abstraction by basic surface oxygen located at defect sites has been proposed [16], which would leave two OH groups at the surface. Direct recombinative desorption of H_2 is intuitively not the most likely path for hydrogen removal. An alternative would be desorption in the form of H_2O under consumption of surface oxygen. Reoxidation could be possible by dissociative adsorption of water or oxygen added to the feed (Mars–Van Krevelen mechanism). However, it has been shown that this stoichiometric reaction would result in a much faster substrate reduction than actually observed [7]. Since the actual mechanism is unknown so far, the dehydrogenation of ethylbenzene to styrene is formally regarded as a single-step surface reaction (Eq. (7)). The hydrogen formed is assumed to be directly released to the gas atmosphere:

$$\mathrm{EB}^{*} \rightarrow \mathrm{St}^{*} + \mathrm{H_2}, \tag{7}$$

on iron oxide and coke.

Styrene is indicated as the precursor of coke formation [22,23] (Eq. (8)). According to [22], the carbonaceous deposits are of a polyaromatic nature, with a H/C ratio of 0.5:

$$\mathrm{St}^{*} \rightarrow \mathrm{coke} + 2\mathrm{H_2}, \tag{8}$$

on iron oxide and coke.

Our own analyses with Auger electron spectroscopy suggest a graphitic structure of the carbonaceous surface layer.

The redox reactions of the iron oxides are formally described by Eqs. (9) and (10). Hydrogen oxidation or water dissociation as the reverse reaction is taken into account implicitly through their linear dependency on Eqs. (9) and (10). This is justified by the high rates of these reaction steps:

$$3\mathrm{Fe_2O_3} + \mathrm{H_2} \rightarrow 2\mathrm{Fe_3O_4} + \mathrm{H_2O}, \tag{9}$$

$$4\mathrm{Fe_3O_4} + \mathrm{O_2} \rightarrow 6\mathrm{Fe_2O_3}. \tag{10}$$

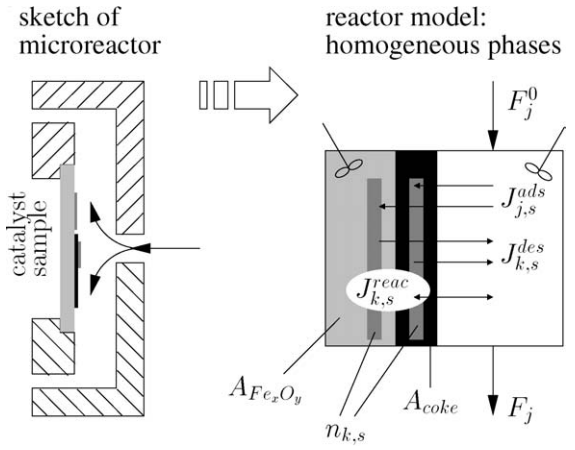

Fig. 2. Reactor model underlying the kinetic modelling. Left: sketch of the microreactor developed for kinetic measurements [19]. Right: reactor model indicating the phases considered.

Removal of coke by gasification in a water vapour- or oxygen-containing atmosphere completes the reaction scheme:

$$\text{coke} + 8H_2O \rightarrow 8CO + 10H_2, \tag{11}$$

$$\text{coke} + 5O_2 \rightarrow 8CO + 2H_2O. \tag{12}$$

3. Model equations

The kinetic reactor used for conversion measurements over monocrystalline model surfaces is described in [21]. Its design is intended to establish a stagnation point flow pattern in the chamber above the catalyst sample. A simple continuous stirred tank reactor (CSTR) model is used to describe the setup in the present context (Fig. 2). This is justified by the low conversions obtained during the kinetic measurements (max. 10%), producing only slight changes in the composition of the reaction mixture. This assumption is also consistent with the observed uniform surface composition during conversion experiments. Furthermore, constant temperature and pressure are assumed. Hence, the model consists of dynamic mass balances of the gaseous, adsorbed, and solid-phase components. Two parallel reaction paths with different rates are considered for the reactions (1)–(8) over coke and iron oxide, as discussed in the previous section.

The total surface areas covered by coke and iron oxide are given by

$$A_{\text{coke}} = N_{\text{coke}} a_{\text{coke}}, \quad a_{\text{coke}} = \text{const.},$$

$$A_{\text{Fe}_x\text{O}_y} = A_0 - A_{\text{coke}}, \quad A_0 = \text{const.},$$

where a_{coke} specifies the molar surface density of the coke layer. Its thickness on the deactivated catalyst was estimated to be about 10 Å by Auger electron spectroscopy. Assuming the atomic density of graphite, this corresponds to about three monolayers. A_0 is the total surface area given by the geometry of the catalyst sample.

The iron oxide surface is assumed to be a pseudo-homogeneous solid since oxygen is known to have a high mobility in the lattice at reaction temperature [24]. Conversion of hematite to magnetite is described through a uniform, continuous depletion of oxygen, and the reverse reaction by a similar addition of oxygen. Accordingly, the iron oxide surface model is represented through a pseudo-component varying continuously between magnetite and hematite. The fraction of each oxide is back-calculated from the oxygen/iron ratio of the pseudo-homogeneous phase. Molar balances of the lattice elements yield the hematite fraction:

$$x_{\text{Fe}_2\text{O}_3} = \frac{3N_{\text{O}} - 4N_{\text{Fe}}}{N_{\text{O}} - N_{\text{Fe}}}, \quad N_{\text{Fe}} = \text{const.}, \tag{13}$$

where N_{Fe} is the constant number of moles of iron in the catalyst sample and N_{O} is the number of moles of lattice oxygen, which is variable. The activity of the iron oxide is variable, depending on the hematite and magnetite content.

The balance equations are expressed in moles. The unknowns of the system N, the number of moles of each component, are coupled through mass exchange terms J.

The balances of gaseous components are calculated as

$$\frac{\mathrm{d}N_j}{\mathrm{d}t} = F_j^0 - F_j - \sum_s J_{j,s}^{\text{ads}} + \sum_s J_{j,s}^{\text{des}} + \sum_i \nu_{i,j} J_i^{\text{reac}},$$
$$i \in \{(j,s),(k,s),p\}.$$

The balances of adsorbed species are calculated as

$$\frac{\mathrm{d}N_{k,s}}{\mathrm{d}t} = J_{k,s}^{\text{ads}} - J_{k,s}^{\text{des}} + \sum_i \nu_{i,k} J_i^{\text{reac}}, \quad i \in \{(k,s)\}.$$

The solid-phase balances are calculated as

$$\frac{\mathrm{d}N_s}{\mathrm{d}t} = \sum_i \nu_{i,s} J_i^{\text{reac}}, \quad i \in \{(j,s),(k,s),p\},$$

$$j \in \{\text{He}, H_2O, \text{EB}, \text{St}, H_2, O_2, \text{CO}\},$$

$$k \in \{\text{EB}^*, \text{St}^*, H_2O^*\},$$

$$s \in \{\text{Fe}_x\text{O}_y, \text{coke}\}, \quad p \in \{Fe_2O_3, Fe_3O_4\}.$$

The balance of the solid pseudo-component iron oxide is expressed in terms of number of moles of lattice oxygen.

The constant-pressure condition of the gas phase yields an expression of the outlet molar flow in terms of the feed stream and the mass exchange streams:

$$\frac{\mathrm{d}N^{\text{gas}}}{\mathrm{d}t} = 0 \Rightarrow F = F^0 - \sum_k \sum_s J_{k,s}^{\text{ads}} + \sum_k \sum_s J_{k,s}^{\text{des}} + \sum_i \sum_j \nu_{i,j} J_i^{\text{reac}}$$

All exchange and conversion streams must be expressed as functions of the unknowns to obtain a well-defined system.

Adsorption and desorption streams are defined for EB, St, and H_2O according to stoichiometric Eqs. (1)–(6). For all other components they are explicitly set to zero.

Adsorption is assumed to be nonactivated and nondissociative, with sticking coefficients $\sigma_{j,s}$ equal to unity:

$$J_{j,s}^{\text{ads}} = \frac{p_j}{(2\pi RTM_j)^{1/2}}\sigma_{j,s}(1-\Theta_s)A_s,$$
$$j \in \{\text{EB}, \text{St}, \text{H}_2\text{O}\}, \quad s \in \{\text{Fe}_2\text{O}_3, \text{Fe}_3\text{O}_4, \text{coke}\},$$

$$\Theta_s = \frac{\sum_k n_{k,s}}{n_s^{\text{sat.}}}, \quad n_{k,s} = \frac{N_{k,s}}{A_s},$$
$$n_s^{\text{sat.}} = \text{const.}, \quad k \in \{\text{EB}^*, \text{St}^*, \text{H}_2\text{O}^*\},$$

where $n_s^{\text{sat.}}$ is the maximum surface concentration of components on the surfaces. In [17] the respective values for EB, St, and H_2O on a magnetite surface were derived theoretically and compared with experimental findings. We assume equal maximum surface concentrations for all components on magnetite and on hematite.

Desorption kinetics are derived from thermal desorption mass spectroscopy (TDS) and can be described by the following expression:

$$J_{k,s}^{\text{des}} = f_{k,s}\mathrm{e}^{\{-E_{k,s}^{\text{des}}/RT\}}n_{k,s}A_s,$$
$$k \in \{\text{EB}^*, \text{St}^*, \text{H}_2\text{O}^*\}, \quad s \in \{\text{Fe}_2\text{O}_3, \text{Fe}_3\text{O}_4, \text{coke}\}.$$

The reaction steps postulated in Eqs. (7)–(12) are considered as single-step reactions. Accordingly, the reaction streams are written as follows:
gasification reactions involving gas-phase components:

$$J_{j,s}^{\text{reac}} = k_{j,s}^0\mathrm{e}^{\{-E_{j,s}^{\text{reac}}/R(\frac{1}{T}-\frac{1}{T_0})\}}A_s p_j,$$
$$j \in \{\text{H}_2\text{O}, \text{O}_2\}, \quad s \in \{\text{coke}\},$$

surface reactions involving adsorbed species:

$$J_{k,s}^{\text{reac}} = k_{k,s}^0\mathrm{e}^{\{-E_{k,s}^{\text{reac}}/R(\frac{1}{T}-\frac{1}{T_0})\}}n_{k,s}A_s,$$
$$k \in \{\text{EB}^*, \text{St}^*\}, \quad s \in \{\text{Fe}_2\text{O}_3, \text{Fe}_3\text{O}_4, \text{coke}\}.$$

Finally, the fluxes related to the phase transformation of either iron oxide to the other by reduction and oxidation are derived based on the principle of nonequilibrium thermodynamics [25]. According to this principle, equilibrium composition of the Fe–O system in the solid phase is determined by the composition of the gas atmosphere. The kinetics follow linear driving force relations, where the chemical affinity of the reaction, X, is assumed to be the driving force [25]:

$$J_p^{\text{reac}} = \left(-\sum_q L_{p,q}\frac{X_q}{T}\right)x_p,$$
$$p \in \{\text{Fe}_2\text{O}_3, \text{Fe}_3\text{O}_4\}, \quad q \in \{\text{H}_2, \text{O}_2,$$
$$X_q = \sum_l \nu_{l,q}\mu_l, \quad l \in \{\text{Fe}_2\text{O}_3, \text{Fe}_3\text{O}_4, \text{H}_2\text{O}, \text{H}_2, \text{O}_2\};$$

$$\mu_l = \mu_l^0(p_0, T) + RT\ln(a_l),$$
$$\begin{cases} a_l = 1, & l = \text{Fe}_2\text{O}_3, \text{Fe}_3\text{O}_4, \\ a_l = p_l/p_0, & l = \text{H}_2\text{O}, \text{H}_2, \text{O}_2. \end{cases}$$

Finally, the individual interactions on hematite and magnetite must be replaced by a single mass exchange term for the balance equations. A lever arm rule applies for the overall interactions of the gas phase with the iron oxide surface:

$$J_{m,\text{Fe}_x\text{O}_y}^{\text{ads/des/reac}} = J_{m,\text{Fe}_2\text{O}_3}^{\text{ads/des/reac}}x_{\text{Fe}_2\text{O}_3} + J_{m,\text{Fe}_3\text{O}_4}^{\text{ads/des/reac}}(1-x_{\text{Fe}_2\text{O}_3}),$$
$$m = \{\text{EB}, \text{St}, \text{H}_2\text{O}, \text{EB}^*, \text{St}^*, \text{H}_2\text{O}^*\}.$$

4. Parameter determination and discussion

The overall set of physico-chemical interactions of the catalyst model shown in Fig. 1 includes in total 31 parameters as introduced in the previous section. Some of them (12 parameters, i.e., the frequency factors and energies for desorption of EB, St, and H_2O from hematite and magnetite) are directly measurable [16–18].

The desorption energy of ethylbenzene over carbonaceous species is directly determined from recent measurements [26]. The respective parameter values for styrene are derived based on the assumption of identical frequency factors and slightly higher activation energy than for ethylbenzene, similar to the findings on different iron oxide surfaces [17]. The parameters of water desorption from coke are determined analogously. The set of desorption parameters is summarised in Table 2.

The parameter values determined for pure components also hold for the reactive system under the assumption of insignificant multicomponent interactions of adsorbed species. This is justified by the low surface coverage under the conditions of the conversion experiments [14].

The remaining 13 parameters have been adjusted to conversion experiments in the kinetic reactor [19–21]. Three test series have been considered for parameter fitting: nonoxidative dehydrogenation over an initially clean magnetite surface (Fig. 3); nonoxidative dehydrogenation over an initially clean hematite surface (Fig. 4); oxidative dehydrogenation over an initially clean hematite surface (Fig. 6).

The conversion measurements have been performed mainly at a temperature of 870 K and a total pressure of 1 bar [7,19]. Experimental data at varying temperatures have been acquired so far for the subsystem 2 (Fig. 5). The available experimental data are gas-phase concentrations measured by gas chromatography (GC) and data from off-line surface analyses. The surface analysis data are labelled in the conversion diagrams. Table 1 summarises the iron oxide fractions derived from Auger electron spectroscopy (AES) and low-energy electron diffraction (LEED). The surface fraction covered by coke is determined by AES and temperature-programmed oxidation (TPO) [19]. These experimental data

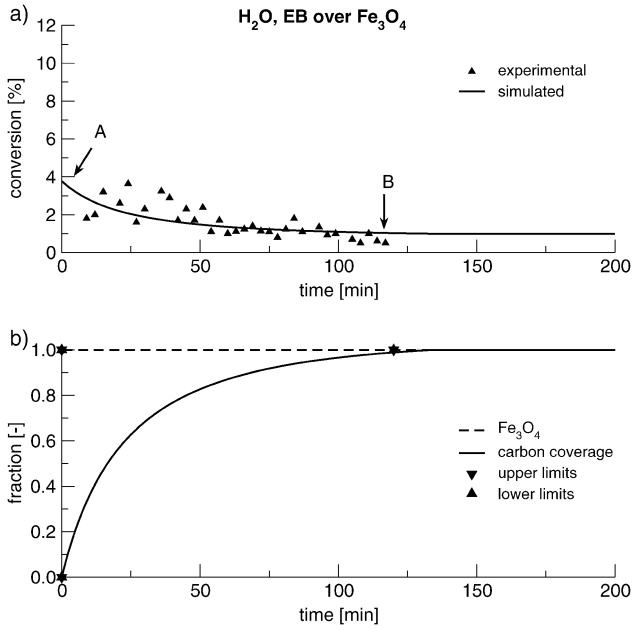

Fig. 3. Experimental basis of subsystem 1 for adjusting the parameters of the kinetic model (symbols) and simulation results (lines). (a) Evolution of conversion with time of pure dehydrogenation over a surface initially consisting of magnetite. (b) Surface composition and coverage by carbon deposits over time. Conditions: $T = 870$ K, $p_{tot} = 1$ bar, $p_{H_2O} = 3400$ Pa, $p_{EB} = 340$ Pa, He carrier gas, $V = 25 \times 10^{-6}$ Nm^3/min.

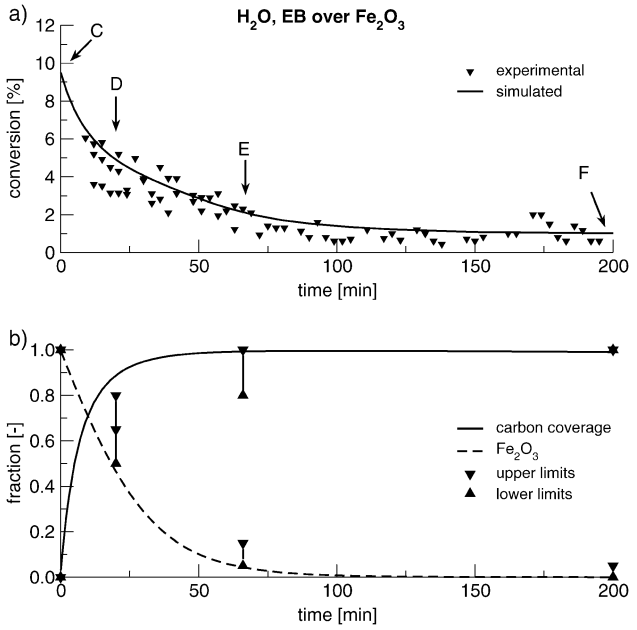

Fig. 4. Experimental basis of subsystem 2 for adjusting the parameters of the kinetic model (symbols) and simulation results (lines). (a) Evolution of conversion with time of pure dehydrogenation over a surface initially consisting of hematite. (b) Surface composition and coverage by carbon deposits over time. Conditions: $T = 870$ K, $p_{tot} = 1$ bar, $p_{H_2O} = 3400$ Pa, $p_{EB} = 340$ Pa, He carrier gas, $V = 25 \times 10^{-6}$ Nm^3/min.

form the basis for fitting the unknown parameters of the kinetic model stated above.

We apply a stepwise parameter fitting procedure, which addresses the different subsystems. The advantage of this strategy is that only a reduced number of interactions are active at the same time and artificial cross-correlations between parameters can be avoided.

The starting point of the parameter fitting is the behaviour of a water–ethylbenzene feed over magnetite model catalysts (Fig. 3). All interactions related to the hematite surface are inactive. Furthermore, no phase change takes place, as no oxygen is present. The change in conversion over time is attributed to coke formation. Surface analysis by AES and TPO clearly indicates complete coverage of the surface with coke (labels B and F) [19]. The evolution of conversion with time and the buildup of carbon deposits allows for determination of the values of k_{EB^*,Fe_3O_4}, k_{St^*,Fe_3O_4}, $k_{EB^*,coke}$, $k_{St^*,coke}$, and $k_{H_2O,coke}$. Fig. 3 indicates the decrease in conversion directly related to the increasing surface coverage by coke. The steady-state conditions at the end of the experiment correlate with the activity of the carbon deposits only.

Next, a water–ethylbenzene feed over hematite is considered (Fig. 4). Processing this data set provides the values of the parameters k_{St^*,Fe_2O_3}, $k_{Fe_2O_3,H_2}$, and $k_{Fe_3O_4,H_2}$. Moreover, conversion measurements over hematite at different temperatures are available for the determination of activation energy $E^{reac}_{EB^*,Fe_2O_3}$ and the pre-exponential factor k_{EB^*,Fe_2O_3} on hematite. Fig. 5 depicts the measured conversion at three different temperatures along with the simulated values.

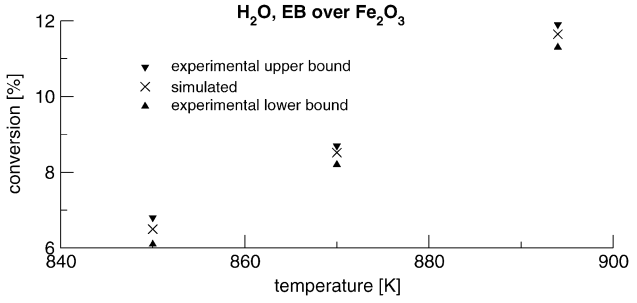

Fig. 5. Experimental basis of subsystem 2 for adjusting the parameters of the kinetic model and simulation results. Temperature dependent initial conversion of pure dehydrogenation on a clean hematite surface. Conditions: $p_{tot} = 1$ bar, $p_{H_2O} = 3400$ Pa, $p_{EB} = 340$ Pa, He carrier gas, $V = 25 \times 10^{-6}$ Nm^3/min.

Table 1
Iron oxide composition and degree of surface coverage by carbonaceous deposits (both from surface analysis) and measured conversion over epitactically grown, mono-crystalline surfaces at 870 K, $p_{tot} = 1$ bar, $p_{H_2O} = 3400$ Pa, $p_{EB} = 340$ Pa, He carrier gas, $V = 25 \times 10^{-6}$ Nm^3/min.

Identifier	Iron oxide composition		Coke deposition	Conversion
	$X_{Fe_2O_3}$ (–)	$X_{Fe_3O_4}$ (–)	Θ_{coke} (–)	X_{EB} (–)
A	0.0	1.0	0.0	3.5
B	0.0	1.0	1.0	0.95
C	1.0	0.0	0.0	9.0
D	0.50–0.65	0.35–0.50	0.5–0.8	–
E	0.05–0.15	0.85–0.95	> 0.8	–
F	< 0.05	> 0.95	1.0	0.95
G	> 0.80	< 0.20	< 0.5	–

Table 2
Stoichiometric equations considered and parameters for corresponding rate equation

Desorption	Surface	$f_{k,s}$ (s^{-1})	$E^{des}_{k,s}$ (J/mol)	Reference
$EB^* \rightarrow EB + {}^*$	Fe_2O_3	1×10^{12}	64×10^3	[16]
	Fe_3O_4	1×10^{12}	86×10^3	[16]
	Coke	5×10^{14}	65×10^3	[26]
$St^* \rightarrow St + {}^*$	Fe_2O_3	5×10^{12}	73×10^3	[16]
	Fe_3O_4	3×10^{11}	118×10^3	[16]
	Coke	5×10^{14}	70×10^3	[26]
$H_2O^* \rightarrow H_2O + {}^*$	Fe_2O_3	1×10^{13}	63×10^3	[18]
	Fe_3O_4	1.0×10^{-5}[a]	65×10^3	[17]
	Coke	1×10^{12}	50×10^3	[26]
Surface reaction	**Surface**	$k^0_{j,s}$ (s^{-1})	$E^{react}_{j,s}$ (J/mol)	**Reference**
$EB^* \rightarrow St^* + H_2$	Fe_2O_3	2.1×10^2	1.6×10^5	this work
	Fe_3O_4	$k(870\ K) = 9.07 \times 10^3\ s^{-1}$		this work
	Coke	$k(870\ K) = 1.53 \times 10^5\ s^{-1}$		this work
$St^* \rightarrow coke^* + 2H_2$	Fe_2O_3	$k(870\ K) = 1.08 \times 10^1\ s^{-1}$		this work
	Fe_3O_4	$k(870\ K) = 1.42 \times 10^{-1}\ s^{-1}$		this work
	Coke	$k(870\ K) = 1.70 \times 10^1\ s^{-1}$		this work
Gas–solid–reaction		$k(T)$ (mol/(s cm^2))		**Reference**
$Coke^* + 8H_2O \rightarrow 8CO + 10H_2$		$k(870\ K) = 1.42 \times 10^{-13}$		this work
$Coke^* + 5O_2 \rightarrow 8CO + 2H_2O$		$k(870\ K) = 1.76 \times 10^{-9}$		this work
Phase transformation		$L_{p,1}$ (mol^2 K/(J s))	$L_{p,2}$ (mol^2 K/(J s))	**Reference**
$3Fe_2O_3 + H_2 \rightarrow 2Fe_3O_4 + H_2O$		1.5×10^{-13}	1.0×10^{17}	this work
$4Fe_3O_4 + O_2 \rightarrow 6Fe_2O_3$		1.0×10^{-17}	1.3×10^{-13}	this work

[a] (cm^2/s) due to second order relation $J^{des}_{k,s} = J^{des}_{k,s}((nk,_s)^2)$.

Finally, the addition of oxygen to the process is considered (Fig. 6). Starting from hematite, all interactions become active and allow for the determination of the remaining parameters, $k_{O_2,coke}$, $k_{Fe_2O_3,O_2}$, and $k_{Fe_3O_4,O_2}$. The complete set of the model parameters is summarised in Table 2.

Fig. 7 presents an energy diagram displaying activation energies of the steps occurring during transformation from ethylbenzene to styrene. The adsorption energies of ethylbenzene and styrene are experimentally verified. The estimated value of the apparent activation energy of the conversion of adsorbed ethylbenzene to styrene (Eq. (7)) is thermodynamically consistent.

The kinetic model is validated by application of the dynamic response of the system to a step-change of the feed composition. The experiment starts with a fresh hematite model catalyst and a feed stream of water, ethylbenzene, and oxygen. After 120 min the oxygen supply is interrupted for 30 min. Fig. 8 shows excellent agreement between the measured and simulated conversion.

We conclude that the catalyst model and the used parameter set adequately describe the behaviour of the styrene synthesis process over ideal, monocrystalline surfaces that are free from mass transport limitations. The model also describes the observed catalyst deactivation, taking into account transformations of the catalyst phase and the formation of carbonaceous deposits. The validity of the set of pa-

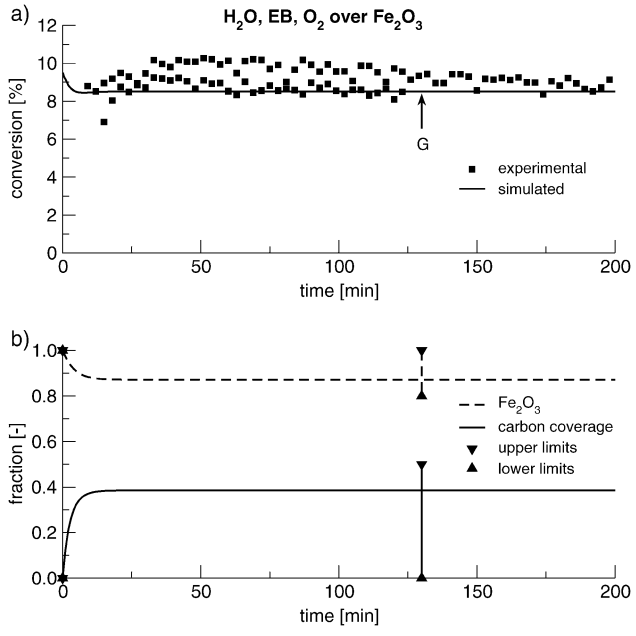

Fig. 6. Experimental basis of the complete system for adjusting the parameters of the kinetic model (symbols) and simulation results (lines). (a) Evolution of conversion with time of dehydrogenation in presence of oxygen over a surface initially consisting of hematite. (b) Surface composition and coverage by carbon deposits over time. Conditions: $T = 870$ K, $p_{tot} = 1$ bar, $p_{H_2O} = 3400$ Pa, $p_{EB} = 340$ Pa, $p_{O_2} = 190$ Pa, He carrier gas, $V = 25 \times 10^{-6}$ Nm^3/min.

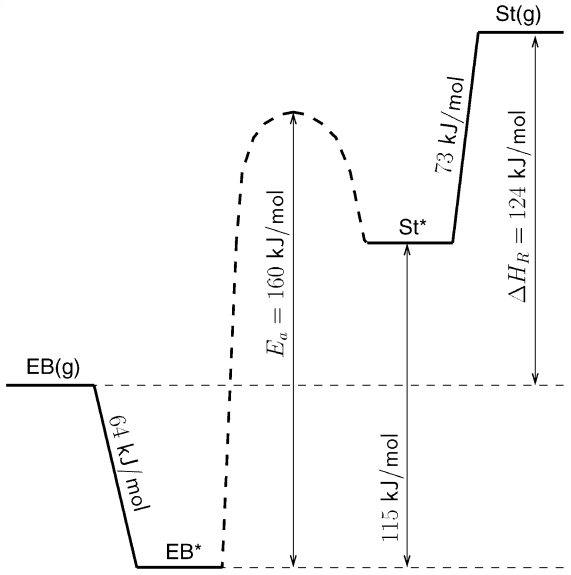

Fig. 7. Energy diagram of activation energies for the overall transformation from ethylbenzene to styrene on hematite.

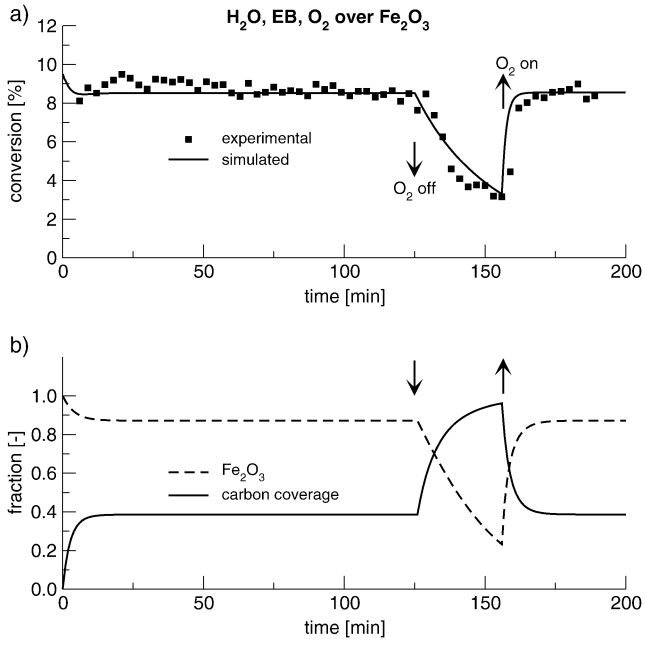

Fig. 8. Validation experiment for the kinetic model (symbols) and simulation results (lines). ↓: switching off oxygen in the feed; ↑: switching on oxygen in the feed. Conditions: $T = 870$ K, $p_{tot} = 1$ bar, $p_{H_2O} = 3400$ Pa, $p_{EB} = 340$ Pa, $p_{O_2} = 190$ Pa, He carrier gas, $V = 25 \times 10^{-6}$ Nm^3/min.

rameters is confirmed by the fact that parameters derived for independent subsystems could be adopted unchanged for the description of the full system. An *a posteriori* confirmation of the chosen stepwise approach is given by the sensitivity analysis with respect to the adjustable parameters presented in Appendix A.

5. Conclusions and outlook

A mechanistic model for the dehydrogenation of ethylbenzene to styrene over single crystal iron oxide films is derived and parameterised based on a combined surface science and chemical engineering approach. The experimental data used for parameter fitting originate from TDS measurements in ultrahigh vacuum and conversion measurements in a microreactor. The conversion measurements comprise the transient behaviour of increasingly complex subsets of the considered reaction system. In addition, off-line surface analysis by LEED, AES, and TPO provides insight into surface composition and coverage by carbon deposits.

A stepwise procedure has been applied to determine the parameters of the kinetic model following the order of the conversion experiments. An excellent agreement between modelling and experimental results is attained. The results confirm that the behaviour of the single crystalline surface can be described with a continuum model as a function of macroscopic variables (catalyst composition, gas-phase composition, surface coverage). Hence, the model is compatible with commonly used reactor models in chemical engineering and can be regarded as the first step towards utilizing the knowledge gained from analyses of the ideal system under well-defined conditions to understand and model technical catalysts. In a next step the focus will be on modelling porous catalysts and assessing whether they can be described adequately by the superposition of the above kinetic model, valid for the single crystal surface, and an adequate pore model accounting for diffusional transport.

Acknowledgments

We acknowledge the financial support of the Deutsche Forschungsgemeinschaft (KO2049/2-2 and RA376/2-2). Our special thanks go to Prof. G. Eigenberger and Prof. G. Veser.

Appendix A

Sensitivity analysis provides a compact and simplified picture of the significance of the model parameters for the residual of the optimisation problem. Sensitivity diagrams display the dependence of a characteristic on the significant parameters. The characteristic is usually a quantity of practical relevance derived from the state variables of the model, such as conversion, yield or selectivity. However, the selection of the characteristic and its normalisation imposes a certain arbitrariness on sensitivity analysis. To reduce arbitrariness to a minimum, the sensitivity analysis presented in the following uses the norm of the residual vector as a characteristic. The residual vector of the optimisation problem underlying the parameter fitting procedure includes information on ethylbenzene conversion, coke coverage, and

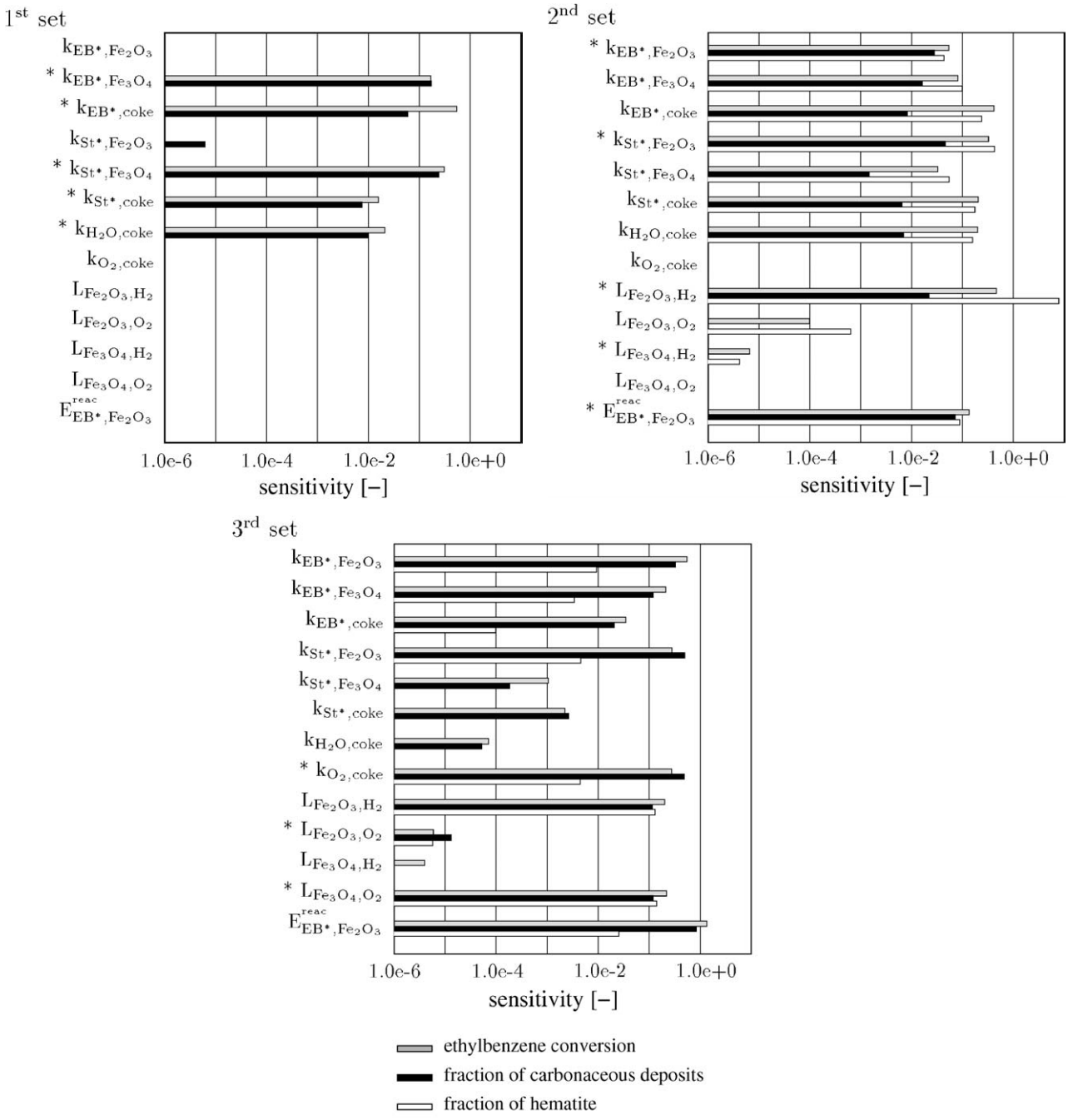

Fig. 9. Sensitivity diagrams corresponding to the three steps of parameter fitting procedure.

hematite fraction of the iron oxide surface. These quantities are used as characteristics in the following analysis. The sensitivity is generally defined as follows:

$$S_{i,j}(t) = \frac{(\Phi_i(k_j^{\mathrm{ref}} + \Delta k_j, t) - \Phi_i(k_j^{\mathrm{ref}}, t))k_j^{\mathrm{ref}}}{\Phi_i(k_j^{\mathrm{ref}}, t)\Delta k_j}$$

$\Phi_i = \{X_{\mathrm{EB}}, N_{\mathrm{coke}}, x_{\mathrm{Fe_2O_3}}\}$ represents the characteristic and k_j the adjustable parameter. The characteristic is obviously time dependent. Therefore, the mean value of the R^1-norm is computed over the measurement interval of an experimental run:

$$\bar{S}_{i,j} = \frac{1}{t_{\mathrm{end}} - t_{\mathrm{begin}}} \int_{t_{\mathrm{begin}}}^{t_{\mathrm{end}}} |S_{i,j}(t)|\,\mathrm{d}t.$$

Fig. 9 displays the sensitivity diagrams corresponding to the three experimental series used for parameter fitting (corresponding to Figs. 3, 4, and 5). The sensitivities of the three

characteristics are included in each diagram. The parameters adjusted to the respective experimental run are indicated by a star. Clearly, the model is sensitive with respect to the parameters assigned to each subsystem.

Appendix B. Nomenclature

N	number of moles of a component (mol)
N_{Fe}	number of moles of iron in the catalyst sample; 6.55×10^{-8} mol
J	component mass exchange terms (mol/s)
F	flow (mol/s)
$n_{\mathrm{s}}^{\mathrm{sat.}}$	molar surface specific concentration of adsorbed species; 332.23×10^{-12} mol/cm^2
a_{coke}	molar surface area of carbonaceous deposits; 1.143×10^{9} cm^2/mol
A_0	total surface area; 0.50 cm^2
A	surface area (cm^2)
p	partial pressure of gas-phase component (Pa)
T	temperature (K)
R	general gas constant (J/(mol K))
M	molar mass of gas-phase component (g/mol)
σ	sticking coefficient of gas-phase component in adsorption relation; all equal to 1.0 (–)
Θ	surface coverage (–)
E	activation energy (J/mol)
f	frequency factor of surface species in desorption relation (s^{-1})
k^0	frequency factor of surface reaction (s^{-1})
T_0	threshold temperature in surface reaction relation; 773.0 (K)
L	frequency factors in phase transformation relation (mol^2 K/(J s))
ν	stoichiometric coefficient of redox reactions of the iron oxides (–)
μ	chemical potential of component in phase transformation relation (J/mol)
x	molar fraction of iron oxide (mol/mol)

Subscripts

j	gas-phase component
k	adsorbed species
s	surface species
i	surface reaction
l	specie participating in redox reaction
p	iron oxide reactant of redox reaction
q	gas-phase reactant of redox reaction

Superscripts

0	inlet
gas	gas phase
ads	adsorption
des	desorption
reac	reaction

References

[1] J.A. Dumesic, D.F. Rudd, L.M. Aparicio, J.E. Rekoske, A.A. Trevino, The Microkinetics of Heterogeneous Catalysis, American Chemical Society, Washington, DC, 1993.
[2] G. Ertl, J. Vac. Sci. Technol. A 1 (1983) 1247.
[3] P. Stoltze, J.K. Norskov, Phys. Rev. Lett. 55 (1985) 2502.
[4] M. Bowker, I.B. Parker, K.C. Waugh, Appl. Catal. 14 (1985) 101.
[5] R. Schlögl, in: G. Ertl, J. Knözinger, J. Weitkamp (Eds.), in: Handbook of Heterogeneous Catalysis, vol. 4, VCH, Weinheim, 1997, Chap. 2.1.
[6] G.R. Meima, P.G. Menon, Appl. Catal. A 212 (2001) 239.
[7] O. Shekhah, W. Ranke, A. Schüle, G. Kolios, R. Schlögl, Angew. Chem. Int. Ed. 42 (2003) 5760.
[8] N.N. Lebedev, G.V. Odabashyan, V.V. Lebedev, M.G. Makorov, Kinet. Katal. 18 (1978) 1177.
[9] S.S.E.H. Elnashaie, B.K. Abdalla, R. Hughes, Ind. Eng. Chem. Res. 32 (1993) 2537.
[10] G. Kolios, G. Eigenberger, Chem. Eng. Sci. 54 (1999) 2637.
[11] J.D. Snyder, B. Subramaniam, Chem. Eng. Sci. 49 (1994) 5585.
[12] A.A. Savoretti, D.O. Borio, V. Bucala, J.A. Porras, Chem. Eng. Sci. 54 (1999) 205.
[13] M. Muhler, R. Schlögl, G. Ertl, J. Catal. 138 (1992) 413.
[14] S.K. Shaikhutdinov, Y. Joseph, C. Kuhrs, W. Ranke, W. Weiss, Faraday Discussions 114 (1999) 363.
[15] Y. Joseph, W. Ranke, W. Weiss, J. Phys. Chem. B 104 (2000) 3224.
[16] C. Kuhrs, Y. Arita, W. Weiss, W. Ranke, R. Schlögl, Top. Catal. 14 (2001) 111.
[17] W. Ranke, Y. Joseph, Phys. Chem. Chem. Phys. 4 (2002) 2483.
[18] W. Weiss, W. Ranke, Prog. Surf. Sci. 70 (2002) 1.
[19] O. Shekhah, W. Ranke, R. Schlögl, J. Catal. 225 (2004) 56.
[20] W. Ranke, O. Shekhah, Recent Res. Dev. Surf. Sci. 1 (2004) 75.
[21] C. Kuhrs, M. Swoboda, W. Weiss, Top. Catal. 15 (2001) 13.
[22] M. Guisnet, P. Magnoux, Appl. Catal. A 212 (2001) 83.
[23] F.D. Kopinke, G. Zimmermann, G.C. Reyniers, G.F. Froment, Ind. Eng. Chem. Res. 32 (1993) 2620.
[24] B. Amami, M. Addou, C. Monty, Defect and Diffusion Forum 194–199 (2001) 1051.
[25] V.N. Krylov, D.A. Shub, Nonequilibrium Processes in Catalysis, CRC Press, London, 1994, p. 187.
[26] R. Zacharia, Desorption of gases from graphitic and porous carbon surfaces, Dissertation, FU Berlin 2004.